RESEARCH ARTICLE

Macromolecular Rapid Communications
www.mrc-journal.de

Flexible Ink-Jet Printed Polymer Light-Emitting Diodes using a Self-Hosted Non-Conjugated TADF Polymer

Cameron M. Cole, Susanna V. Kunz, Thomas Baumann, James P. Blinco, Prashant Sonar, Christopher Barner-Kowollik, and Soniya D. Yambem**

Thermally activated delayed fluorescent (TADF) emitters have become the leading emissive materials for highly efficient organic light-emitting diodes (OLEDs). The deposition of these materials in scalable and cost-effective ways is paramount when looking toward the future of OLED applications. Herein, a simple OLED with fully solution-processed organic layers is introduced, where the TADF emissive layer is ink-jet printed. The TADF polymer has electron and hole conductive side chains, simplifying the fabrication process by removing the need for additional host materials. The OLED has a peak emission of 502 nm and a maximum luminance of close to 9600 cd m^{-2}. The self-hosted TADF polymer is also demonstrated in a flexible OLED, reaching a maximum luminance of over 2000 cd m^{-2}. These results demonstrate the potential applications of this self-hosted TADF polymer in flexible ink-jet printed OLEDs and, therefore, for a more scalable fabrication process.

1. Introduction

Since Tang and Van Slyke's pioneering work on organic light-emitting diodes (OLEDs), OLEDs have rapidly advanced and are now one of the most promising display technologies.[1] OLEDs have been widely adopted across industry with applications in display technologies ranging from small portable devices to large televisions. Application of OLEDs is also emerging in wearable virtual reality and augmented reality devices. OLEDs are desirable for many reasons. They are lightweight, flexible, thin, and have wide viewing angles.[2]

We are currently in the third generation of OLEDs. The different generations of OLEDs have been influenced by the development of different classes of emissive materials. The first and second generations of OLEDs had fluorescent and phosphorescent materials as emissive layers. Phosphorescent materials can potentially harvest 100% of the electrogenerated excitons, a major advantage compared to fluorescent materials that allow harvesting of only 25% of the electrogenerated excitons, limiting the overall efficiency of the OLEDs.[3] Phosphorescent materials, however, require the presence of rare heavy metal atoms, such as platinum and iridium complexes.[4] This is overcome in the third generation of OLEDs with thermally activated delayed fluorescent (TADF) emitters, which can potentially harvest 100% of the electrogenerated excitons without the use of heavy metal complexes.[5] Furthermore, since the first demonstration of TADF emitters in OLEDs,[6] and the first pure organic TADF molecule in OLEDs,[7] pure organic TADF emitters have reached internal quantum efficiencies (IQEs) of ≈100%.[8]

The predominant fabrication method used in fabricating TADF OLEDs is vacuum deposition. Vacuum deposition is able to achieve TADF OLEDs with high efficiencies through easy layering of functional materials. However, the process of vacuum deposition results in a large loss of material, and size is limited by the deposition chamber. In addition, this process is relatively expensive.[4] A potentially low-cost and simple alternative to vacuum deposition is solution processing. Suitable solution-processing methods that can overcome the abovementioned disadvantages include spin-coating, ink-jet printing, and screen printing, with the latter two being adequate scalable options.[9]

Numerous materials have been developed for solution-processed TADF OLEDs, ranging from small molecules to macromolecules (i.e., dendrimers and polymers), with the latter being developed into self-hosted materials that further benefit solution processing by reducing effects such as aggregation quenching and phase separation.[4,10–14] Although there are countless materials under development for solution-processed TADF OLEDs, only a handful have been demonstrated in TADF

C. M. Cole, S. V. Kunz, J. P. Blinco, P. Sonar, C. Barner-Kowollik, S. D. Yambem
Centre for Materials Science, School of Chemistry and Physics
Queensland University of Technology (QUT)
2 George Street, Brisbane, QLD 4000, Australia
E-mail: christopher.barnerkowollik@qut.edu.au; soniya.yambem@qut.edu.au
T. Baumann
Cynora GmbH
Werner-von-Siemens-Straße 2–6, 76646 Bruchsal, Germany
C. Barner-Kowollik
Institute of Nanotechnology (INT)
Karlsruhe Institute of Technology (KIT)
Hermann-von-Helmholtz-Platz
76344 Eggenstein-Leopoldshafen, Germany

The ORCID identification number(s) for the author(s) of this article can be found under https://doi.org/10.1002/marc.202300015

DOI: 10.1002/marc.202300015

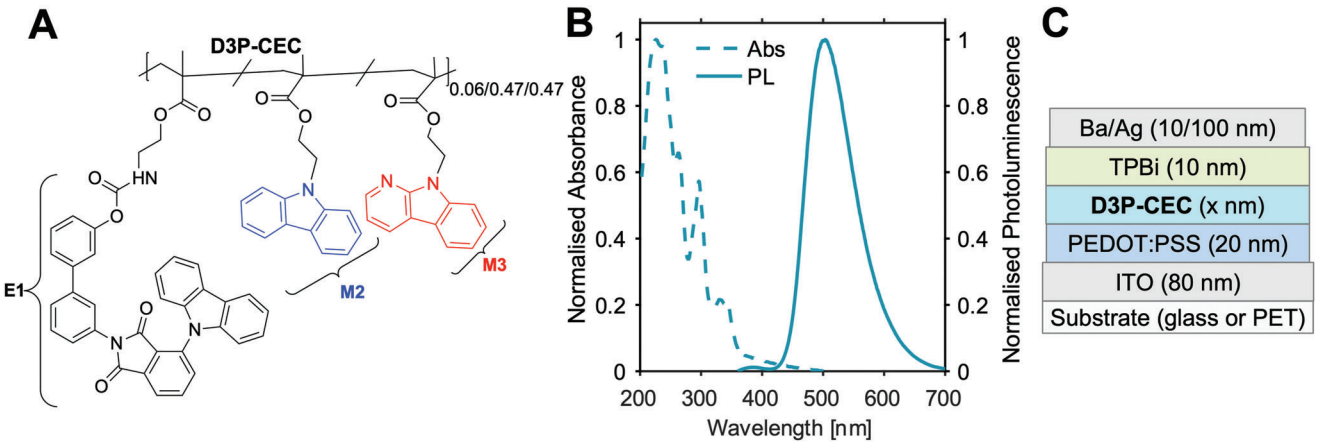

Figure 1. A) Chemical structure of D3P-CEC (M_n ≈30 kDa, $Đ = 3.6$, hole-transporting species are marked in blue and electron-transporting species are marked in red). B) Absorption and photoluminescence (PL) spectrum of D3P-CEC, where the films are excited at 290 nm. C) OLED device structure used for this study which has all solution-processed organic layers.

OLEDs with ink-jet printed emissive layers.[15–19] Furthermore, only a couple of reports are on fully solution-processed organic layers within the OLEDs, one being our earlier work on self-hosted TADF OLEDs.[16,17] Further research into readily processable materials and devices is necessary to further develop pathways toward the scalable fabrication of TADF OLEDs.

Herein, we introduce a flexible ink-jet printed TADF OLED with fully solution-processed organic layers. We employed a self-hosted TADF polymer emitter as the light-emitting layer. This self-hosted TADF polymer is facile to generate based on simplified charge transporting units in the side chains, i.e., α-carboline for the transport of electrons and carbazole for the transport of holes. To the best of our knowledge, our contribution is the first report of a flexible ink-jet printed TADF OLED. Our study is an important contribution toward the simplified fabrication of ink-jet printed TADF OLEDs and contributes to the foundations of large-scale fabrication of flexible TADF OLEDs.

2. Results and Discussion

We recently reported the synthesis of several non-conjugated self-hosted TADF polymers and for the current work on flexible OLEDs, we have chosen the polymer D3P-CEC (**Figure 1**A).[16,20] It has the emitting species 4-(9H-carbazol-9-yl)-2-(3′-hydroxy-[1,1′- biphenyl]-3-yl)-isoindoline-1,3-dione (E1) and two unipolar hosts, carbazole (M2, 46.8 mol.%) and α-carboline (46.8 mol.%) (M3) as pendants in the methacrylate-based polymer chain, with a number average molecular weight of 30 kDa and a dispersity of 3.6. In our earlier report on OLEDs with the self-hosted TADF polymer, D3P-DEH, which has the same emitting species E1, we used two unipolar hosts based on the commercial host materials, 1,3-di(9H-carbazol-9-yl)benzene (mCP).[16] Compared to ambipolar hosts, featuring a combination of two unipolar hosts within the polymer has the advantage of enabling a simpler approach to adjust the balancing of charges by varying the monomer ratios, as well as avoiding the generally low-yielding asymmetric synthesis.[20] For D3P-CEC, the (monomer) synthesis is further simplified through the use of carbazole and α-carboline units as pendant groups replacing more complex hosts such as mCP. Additionally, many of the characteristics (including, importantly, the TADF properties) of D3P-CEC remain unchanged and were very similar to our other self-hosted polymers.[20] The absorption and photoluminescent (PL) spectrum of D3P-CEC is shown in Figure 1B. D3P-CEC has a PL peak emission at 504 nm and a full-width half maximum (FWHM) of 91 nm.

To study D3P-CEC in OLEDs, a simple OLED device structure (Figure 1C) was chosen, where poly(3,4-ethylenedioxythiophene) doped with poly (styrene sulfonate) (PEDOT:PSS) is the hole transporting layer (HTL) and 1,3,5-tris(1-phenyl-1H-benzimidazol-2-yl)benzene (TPBi) is the electron transporting layer (ETL). indium-tin-oxide (ITO) is the anode and barium (Ba)/silver (Ag) is the cathode. All organic layers were deposited through solution processing methods (either spin-coating or ink-jet printing). For OLEDs that are fabricated with multiple solution-processed layers, such as ours, the major challenges when selecting a solvent for spin-coating are the solubility of the material in the solvent to achieve the desired thickness, and the orthogonality of the solvent to the underlying layer. As D3P-CEC is highly soluble in chloroform, and chloroform is an orthogonal solvent to the underlying PEDOT:PSS film, a uniform spin-coated film was achieved, as seen in the atomic force microscopy (AFM) image in Figure S1 (Supporting Information). This spin-coated film on PEDOT:PSS has a root mean square surface roughness (R_q) of 0.374 nm and an average roughness (R_a) of 0.298 nm. On the other hand, although ink-jet printing can result in a much more efficient and scalable option compared to spin-coating, it requires more optimization in a range of areas including ink formulation, substrate properties, and ink-jet printing parameters.[21]

For ink-jet printing, to simplify the fabrication process and reduce the number of steps as well as reduce the number of materials, we opted to use just one solvent, anisole. Anisole is a non-halogenated solvent with low toxicity, which is an important prerequisite when looking forward to potential scalability. While using one solvent simplifies the fabrication process, it can increase the likelihood of several common ink-jet printing issues occurring, such as the coffee-ring effect. The coffee-ring effect happens

when the capillary flow pushes the ink toward the outer sides of the droplet when drying, thus causing a coffee-ring shape. The most common method to reduce the coffee-ring effect is to use a main solvent (lower boiling point and higher surface tension) mixed with a co-solvent (higher boiling point and lower surface tension). By doing so, the outward capillary flow and the inward Marangoni flow are balanced and result in a more homogenous droplet.[22] As we are using a single solvent, we explored other methods to reduce the coffee-ring effect.

Reducing the substrate temperature during ink-jet printing has been shown to reduce the severity of the coffee-ring effect. As the substrate temperature increases, the evaporation rate of the solvent around the thin pinned edges also increases, pulling more solvent and solute toward the edges.[23] This effect can be exacerbated when printing films using a single-nozzle ink-jet printer. In the case of a single nozzle ink-jet printer, the drying time of each individual line needs to be considered, so that the line has not completely dried before the next line is printed next to it to form a uniform film. Thus, print speed and droplet spacing in both directions (x and y) need to be optimized.

Herein, the print-bed and print-head temperatures were set to just above room temperature (25 °C) so that they could be kept at the lowest possible yet consistent temperature throughout the study. D3P-CEC in anisole is printed using a bipolar trapezoidal waveform (Figure S2, Supporting Information). The droplets that were produced from this bipolar waveform had a volume of 14 ± 1 pL, a diameter of 30 ± 1 µm, and were dropping at a speed of 2.2 ± 0.2 m s^{-1} (stroboscopic images of the printed droplet are shown in Figure S2, Supporting Information). Initially, an array with droplet spacings of 70 × 70 µm (x × y direction, where the printer prints along the x direction first) was printed on an ITO/PEDOT:PSS film at print speeds of 5, 15, and 30 mm s^{-1} (**Figure 2**A–C). From the confocal fluorescence images of the prints, horizontal lines are evident in all three prints (Figure 2A–C). The surface profile of these films measured by a stylus profilometer is shown in Figure 2G. The R_q values extracted from the stylus profilometer measurements for films printed at speeds 5, 15, and 30 mm s^{-1} are 6.04, 12.12, and 6.19 nm respectively. However, when a small 5 × 5 µm section of these films (Figure 2A–C) was imaged through atomic force microscopy (AFM), their AFM R_q values are 0.34, 0.36, and 0.40 nm, respectively (Figure S3, Supporting Information). These low AFM R_q values are comparable to those of uniform spin-coated films and indicate that while the printed films have raised edges due to the drying of individual lines in the vertical direction (as seen in the confocal microscopy images), the uniformity of the dried film between these raised edges is promising and suitable for an OLED.

Figure 2C,F compare arrays printed at 30 mm s^{-1} with droplet spacings of either 70 × 70 µm or 50 × 50 µm, respectively. Not only does the print with 50 × 50 µm droplet spacings show less uniformity over the entire imaged area, but the stylus profilometer measurement also shows a much larger R_q (10.3 nm) compared to the 70 × 70 µm array (6.19 nm). Again, the AFM R_q value (0.35 nm) of the 50 × 50 µm droplet spaced film is much lesser and similar to those of 70 × 70 µm droplet spaced films. In Figure 2F, the printed lines can be seen bulging in the vertical direction and the line edges are quite prominent, indicating that the horizontal droplet spacing is too small. To reduce the height of the line edges, the speed was decreased from 30 to 15 mm s^{-1}. A comparison between arrays with 70 × 70 µm print spacings and 70 × 50 µm print spacings, printed at 15 mm s^{-1}, are shown in Figure 2B,E, respectively. It is visible from the confocal images that the 70 × 50 µm print is more uniform with less raised line edges, which is additionally confirmed with the stylus profilometer measurements, where the R_q is reduced from 12.12 to 8.01 nm. Finally, Figure 2D,E show arrays with 70 × 50 µm print spacing printed at speeds of 12.5 or 15 mm s^{-1}, respectively. The reduced print speed of 12.5 mm s^{-1} resulted in further improvement in uniformity with a reduced R_q of 6.19 nm from the stylus profilometer measurements. The AFM image for this film (Figure 2D) is shown in Figure 2H, where the R_q and R_a values are 0.374 and 0.298 nm, respectively. This uniform film with both a low R_q for the stylus profilometer line and AFM was used in all following ink-jet printed OLEDs.

The ink-jet printing parameters, which resulted in the smoothest film (Figure 2D), were subsequently used for printing the emissive layer (EML) of OLEDs (structure shown in Figure 1C and energy level diagram shown in Figure S4, Supporting Information) with glass substrate and compared to an OLED with a spin-coated EML layer. OLED characteristics of both ink-jet printed and spin-coated EMLs are shown in **Figure 3**. The electroluminescent (EL) spectrum of the ink-jet printed OLED is similar, and mostly overlaps with the EL of the spin-coated OLED, with only a slight blue shift (EL peak shift from 519 to 502 nm). This small variation in EL is most likely a result of a change in thickness of the OLED, where the spin-coated OLED has an EML thickness of close to 12 nm and the ink-jet printed OLED has an EML thickness of ≈32 nm. The effect of change in thickness is also evident in the current-voltage-luminance (IVL) characteristics (Figure 3B). The OLED with a spin-coated EML has a much higher current and luminance at lower voltages. It has a turn-on voltage of 6.3 ± 0.1 V, which is ≈2 V lower than the turn-on voltage, of 8.2 ± 0.1 V, for the OLED with an ink-jet printed EML. The spin-coated OLEDs reached a maximum luminance of 2457 ± 555 cd m^{-2} (maximum driving voltage of 10.2 V). While the ink-jet printed OLED does have a lower maximum luminance at the same drive voltage, it could be driven to a much higher voltage (Figure 3B). When driven to 16 V, it reached a maximum luminance of 9619 ± 804 cd m^{-2}, which, to the best of our knowledge, is the highest recorded luminance for an ink-jet printed TADF material to date.

The current efficiency (CE) and external quantum efficiency (EQE) characteristics of both spin-coated and ink-jet-printed OLEDs are shown in Figure 3C. The spin-coated OLEDs had a maximum CE and EQE of 4.9 ± 0.8 cd A^{-1} and 1.5 ± 0.2%, respectively, while the CE and EQE of the ink-jet printed OLEDs reached a maximum of 2.0 ± 0.3 cd A^{-1} and 0.6 ± 0.1%, respectively (Table S1, Supporting Information). The EQE and CE of the spin-coated OLED show significant efficiency roll-off, which has been previously found with devices fabricated using the same emitting species and is also typical of many TADF emitters.[24] While the ink-jet printed OLED requires more voltage to reach the same luminance values as the spin-coated OLED, due to their gentler efficiency roll-off, the current efficiency and EQE of the ink-jet printed OLED is higher than the spin-coated OLED for luminance > ≈2500 cd m^{-2}. A possible explanation for the rapid efficiency roll-off of the spin-coated OLED as compared to the ink-jet-printed OLED is the difference in the thickness of the EMLs.

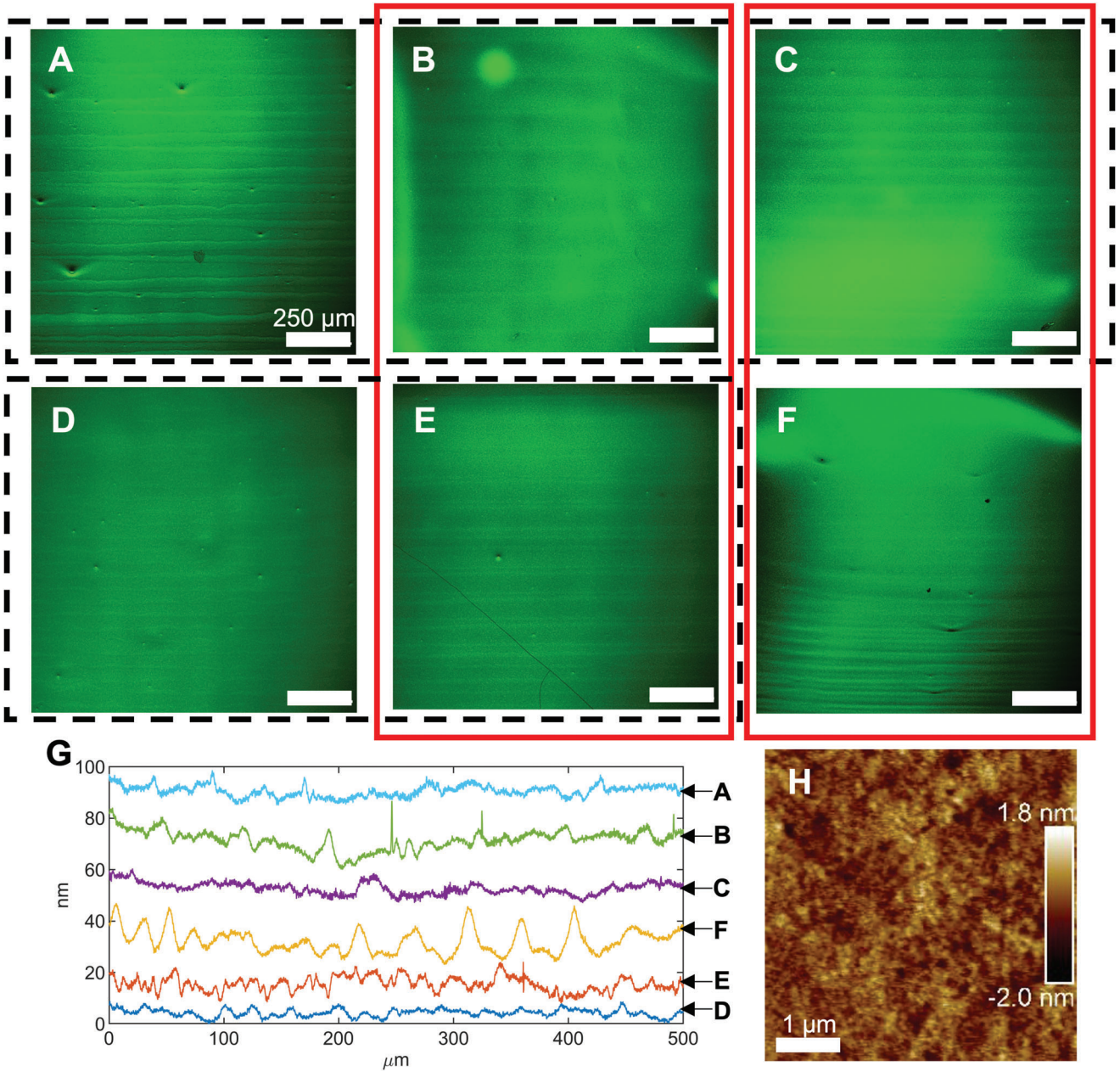

Figure 2. Confocal microscopy images of ink-jet printed D3P-CEC films on ITO/PEDOT:PSS printed at different spacings and speeds. A–C). Printed with 70 × 70 μm spacings at 5, 15, and 30 mm s^{-1}, respectively. D) Printed with 70 × 50 μm spacings at 12.5 mm s^{-1}. E) Printed with 70 × 50 μm spacings 15 mm s^{-1}. F) Printed with 50 × 50 μm spacings at 30 mm s^{-1}. G) Surface profiles (in the vertical direction) of prints (A–F) measured by a stylus profilometer. Prints (A–F) have a root mean square, R_q roughness of 6.04, 12.12, 6.19, 4.58, 8.01, and 10.3 nm, respectively. H) AFM image of ink-jet printed D3P-CEC film on ITO/PEDOT:PSS corresponding to (D) (R_a = 0.298 nm, R_q = 0.374 nm).

Due to the thinner EML of the spin-coated OLEDs, the charge recombination zone for this OLED will be closer to the EML/ETL interface. Thus, exciton quenching may be occurring when the OLED is driven at higher voltages, resulting in rapid efficiency roll-off.[25]

To demonstrate the versatility of D3P-CEC as an emitter in ink-jet printed OLEDs, flexible OLEDs were fabricated on polyethylene terephthalate (PET) substrates. The flexible OLEDs had the same structure as those fabricated on glass. The same printing parameters for ink-jet printing were used for flexible OLEDs. No significant changes in the films are expected because of the substrate since the printing was done on ITO/PEDOT:PSS for both substrates. **Figure 4**A shows a photograph of a flexible ink-jet printed OLED with a pixel turned on. Even under strain, visibly the OLED is emitting uniformly. There is also no visible change in uniformity of emission when OLED is flexed in the opposite direction (Figure S5, Supporting Information). The IVL, current efficiency, and EQE characteristics of the flexible OLED are shown

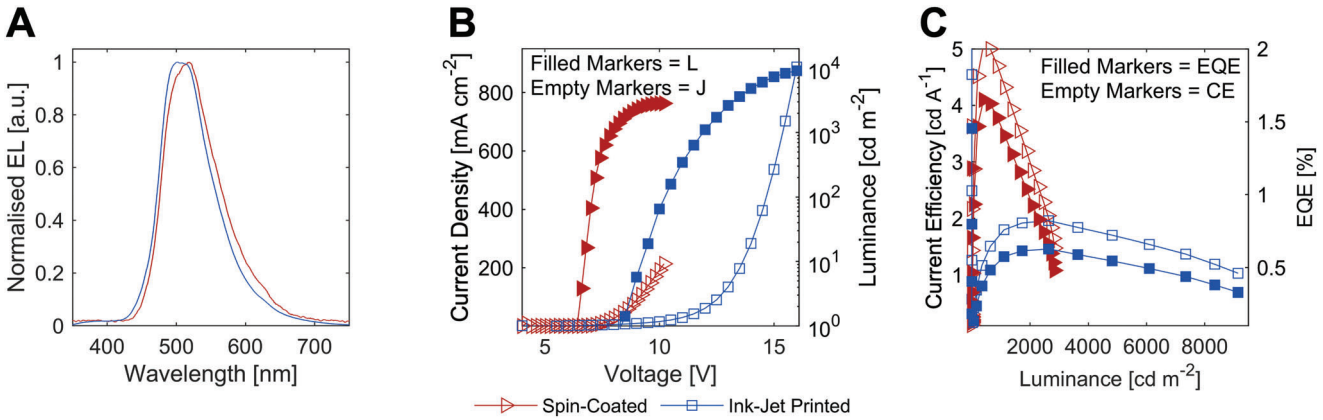

Figure 3. Characteristics of D3P-CEC OLEDs with spin-coated and ink-jet printed EMLs. A) EL spectrum. B) Current density and luminance with respect to voltage. C) Current efficiency (CE) and external quantum efficiency (EQE) with respect to luminance.

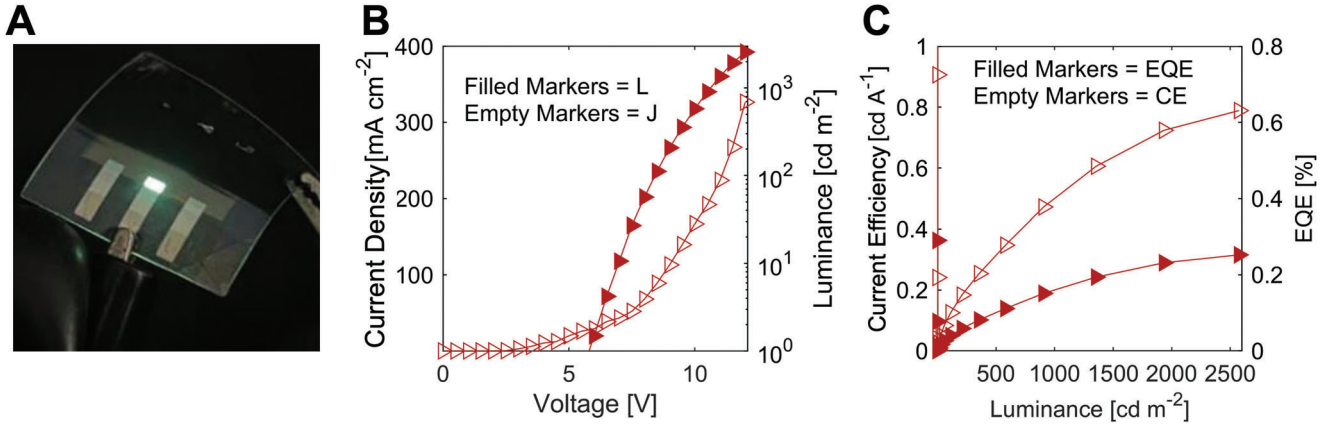

Figure 4. Characteristics of D3P-CEC flexible OLEDs with ink-jet printed EMLs. A) A photograph of ink-jet printed flexible OLEDs with a pixel tuned on. B) Current density and luminance with respect to voltage. C) Current efficiency (CE) and external quantum efficiency (EQE) with respect to luminance.

in Figure 4B,C, respectively. While the flexible ink-jet-printed OLED exhibits lower efficiency, as compared to printed OLEDs on glass substrate, it however reached a luminance of more than 2000 cd m^{-2}. A possible explanation for the decrease in efficiency may be associated with the much higher sheet resistance of the PET/ITO substrate (measured at ≈161 Ω $sq.^{-1}$), compared to the glass/ITO substrate (measured at ≈57 Ω $sq.^{-1}$). Overall, the ink-jet printed OLED data indicates that TADF polymers containing carbazole and α-carboline as pendants are an effective approach toward simple fabrication of flexible ink-jet printed OLEDs.

3. Conclusions

Herein, we demonstrate the use of a TADF polymer, D3P-CEC, with carbazole and α-carboline pendants, as the emissive layer in solution processed OLEDs with a very simple structure, either by spin-coating or ink-jet printing. We show that by optimizing the printing parameters, an ink-jet printed D3P-CEC film with very low roughness values, similar to that of spin-coated films, and suitable for OLEDs was achieved. To the best of our knowledge, our study presents the first flexible ink-jet printed TADF OLED. Furthermore, an ink-jet printed OLED on a glass substrate has resulted in the highest recorded luminance of ≈9000 cd m^{-2} for an ink-jet printed TADF OLED. With future work on implementing D3P-CEC in more intricate device structures, improved brightness and efficiencies could be achieved. In summary, our results show that the use of carbazole and α-carboline host species as pendants on polymers containing TADF emitting materials is an efficient strategy for the scalable fabrication of TADF OLEDs.

4. Experimental Section

The synthesis and characterization of the employed TADF emitter polymer was reported in our earlier work,[20] NMR, CV, and SEC data can be found in the Supporting Information. Additional NMR spectra for the monomers used in D3P-CEC can also be found in the Supporting Information of the previous work.[20]

Patterned substrates with ITO on glass or PET were scrubbed with cotton tips dosed in acetone and then again with cotton tips dosed in a solution of lab detergent (Alconox) in deionized water. All substrates were then ultrasonicated in a solution of the lab detergent for 10 min and dried with compressed air. This step of ultrasonication and drying was repeated in acetone and isopropanol. The cleaned substrates were spin-coated (Laurell Technologies Corporation, WS-650MZ-23NPP) with PEDOT:PSS (Heraeus Clevios, AI 4083) filtered with a 0.45 µm PVDF filter (Kinesis Australia

Pty. Ltd., ESF-PVH-13-045) at 5000 rpm for 30 s to deposit a 21.9 ± 1.1 nm film. Using a cotton tip wetted with deionized water, the ITO contacts were exposed before annealing on a hotplate at 125 °C for 20 min. For the spin-coated OLEDs, the PEDOT:PSS-coated substrates were then transferred into a glove box with low O_2 (<10 ppm) and H_2O (<0.1 ppm). The PEDOT:PSS-coated substrates for the ink-jet printed OLEDs remained in ambient conditions and only entered the glove box system post-ink-jet printing.

For OLEDs with spin-coated EML, 5 mg mL^{-1} solution of the self-hosted TADF polymer (described in results and discussions) in chloroform (Sigma-Aldrich, 288306) was spin-coated at 1500 rpm for 30 s. The contacts were cleaned with chlorobenzene and followed by annealing for 15 min at 60 °C. OLEDs with spin-coated emissive layers were fabricated only on glass substrates.

The ink used for the ink-jet printing of the EML, which had 10 mg mL^{-1} of the TADF polymer in anisole (Sigma-Aldrich, 296295), was prepared inside a glove box and removed for printing. Prior to loading into the printer, the ink was filtered through a 0.22 µm PTFE filter (Kinesis Australia Pty. Ltd., ESF-PT-13-022). A piezoelectric drop-on-demand ink-jet printer (MicroFab, Jet-Lab 4XL) with a single 50 µm print head device was used for all the printing. Once the printing was completed, the printed substrates were annealed for 20 min at 150 °C before being moved into the glove box for the deposition of the final layers and testing.

Following the deposition of the EML, a 4 mg mL^{-1} solution of TPBi (Lumtec, LT-E302) in ethanol (Sigma-Aldrich, 459836) was deposited by spin-coating at 1000 rpm which gave a 22.4 ± 4.2 nm film. The electrical contacts were exposed by wiping off the TPBi with a cotton tip wetted with chlorobenzene. This was followed by annealing for 20 min at 50 °C. Finally, Ba (Sigma–Aldrich, 474711) and Ag (Sigma–Aldrich, 474711) were evaporated using a thermal torpedo evaporator at a pressure of $< 10^{-6}$ mbar and at a rate of < 0.2 Å s^{-1} to deposit a ≈5 nm Ba film and a ≈100 nm Ag film. A mask was used for the Ba/Ag evaporation to yield a 2 mm^2 OLED.

The IVL and EL measurements were conducted inside the glove box. IV and IVL measurements were recorded using a semi-conductor analyzer (Keysight, B1500A) and a calibrated photodiode. A luminance meter (Konica Minolta, CS-200) was used to calibrate the photodiode. The EL spectra were recorded using a UV–vis spectrometer (Ocean Optics, USB 2000+). A minimum of 5 OLEDs were analyzed to calculate the averages.

Images of the ink-jet printed films were taken using a confocal microscope (Nikon, A1R Confocal) at 10 × magnification using a 405 nm DAPI laser. Film roughness measurements were recorded using an AFM (Bruker, Dimension Icon AFM). The AFM data were analyzed using NanoScope Analysis (Bruker). The thin-film thicknesses as well as the topology of the ink-jet printed films were measured using a stylus profilometer (Bruker, Dektak).

The PL and absorption measurements were recorded using a fluorescence spectrometer (Agilent, Cary Eclipse) with an excitation wavelength of 290 nm and a UV–vis (Agilent, Cary 60), respectively. The films were spin-coated onto quartz substrates (Xin Yan Technology Ltd.) for the PL and absorption measurements.

Supporting Information

Supporting Information is available from the Wiley Online Library or from the author.

Acknowledgements

C.B.-K., J.P.B., P.S., and S.D.Y. acknowledged funding in the context of an Australian Research Council (ARC) Linkage project LP170100387. C.B.-K. was grateful for an ARC Laureate Fellowship enabling his photochemical research program, as well as continued key support from the Queensland University of Technology (QUT). P.S. was thankful for an ARC Future Fellowship. The Central Analytical Research Facility (CARF) at QUT was gratefully acknowledged for access to analytical instrumentation. The authors thanked Prof. Eva Blasco, Heidelberg University (Germany), for helpful discussions.

Open access publishing facilitated by Queensland University of Technology, as part of the Wiley - Queensland University of Technology agreement via the Council of Australian University Librarians.

Conflict of Interest

The authors declare no conflict of interest.

Data Availability Statement

The data that support the findings of this study are available from the corresponding author upon reasonable request.

Keywords

flexible electronics, ink-jet printing, organic light-emitting diodes, self-hosted polymers, solution-processability, thermally activated delayed fluorescence polymers

Received: January 11, 2023
Revised: March 5, 2023
Published online: April 26, 2023

[1] C. W. Tang, S. A. Vanslyke, *Appl. Phys. Lett.* **1987**, *51*, 913.
[2] R. Rana, A. Jetly, R. Mehra, in Applications of Computing, Automation and Wireless Systems in Electrical Engineering. *Lecture Notes in Electrical Engineering*, vol. *553* (Eds: S. Mishra, Y. Sood, A. Tomar), Springer, Singapore **2019**.
[3] Y. Liu, C. Li, Z. Ren, S. Yan, M. R. Bryce, *Nat. Rev. Mater.* **2018**, *3*, 18020.
[4] H. J. Kim, C. Lee, M. Godumala, S. Choi, S. Y. Park, M. J. Cho, S. Park, D. H. Choi, *Polym. Chem.* **2018**, *9*, 1318.
[5] Z. Yang, Z. Mao, Z. Xie, Y. Zhang, S. Liu, J. Zhao, J. Xu, Z. Chi, M. P. Aldred, *Chem. Soc. Rev.* **2017**, *46*, 915.
[6] A. Endo, M. Ogasawara, A. Takahashi, D. Yokoyama, Y. Kato, C. Adachi, *Adv. Mater.* **2009**, *21*, 4802.
[7] A. Endo, K. Sato, K. Yoshimura, T. Kai, A. Kawada, H. Miyazaki, C. Adachi, *Appl. Phys. Lett.* **2011**, *98*, 083302.
[8] H. Kaji, H. Suzuki, T. Fukushima, K. Shizu, K. Suzuki, S. Kubo, T. Komino, H. Oiwa, F. Suzuki, A. Wakamiya, Y. Murata, C. Adachi, *Nat. Commun.* **2015**, *6*, 8476.
[9] I. Verboven, W. Deferme, *Prog. Mater. Sci.* **2021**, *118*, 100760.
[10] T. Huang, W. Jiang, L. Duan, *J. Mater. Chem. C* **2018**, *6*, 5577.
[11] S. Wang, H. Zhang, B. Zhang, Z. Xie, W.-Y. Wong, *Mater. Sci. Eng. R* **2020**, *140*, 100547.
[12] J. Rao, L. Yang, X. Li, L. Zhao, S. Wang, H. Tian, J. Ding, L. Wang, *Angew. Chem., Int. Ed.* **2021**, *60*, 9635.
[13] S. Jhulki, M. W. Cooper, S. Barlow, S. R. Marder, *Mater. Chem. Front.* **2019**,*3*, 1699.
[14] W. Zong, W. Qiu, P. Yuan, F. Wang, Y. Liu, S. Xu, S.-J. Su, S. Cao, *Polymer* **2022**, *240*, 124468.
[15] C. M. Cole, S. V. Kunz, P. E. Shaw, N.-P. Thoebes, T. Baumann, E. Blasco, J. P. Blinco, P. Sonar, C. Barner-Kowollik, S. D. Yambem, *J. Mater. Chem. C* **2020**, *8*, 13001.
[16] C. M. Cole, S. V. Kunz, P. E. Shaw, C. S. K. Ranasinghe, T. Baumann, J. P. Blinco, P. Sonar, C. Barner-Kowollik, S. D. Yambem, *Adv. Mater. Technol.* **2022**, *7*, 2200648.
[17] C. Amruth, B. Luszczynska, M. Z. Szymanski, J. Ulanski, K. Albrecht, K. Yamamoto, *Org. Electron.* **2019**, *74*, 218.

[18] A. Verma, D. M. Zink, C. Fléchon, J. Leganés Carballo, H. Flügge, J. M. Navarro, T. Baumann, D. Volz, *Appl. Phys. A* **2016**, *122*, 191.
[19] M. Wallesch, A. Verma, C. Fléchon, H. Flügge, D. M. Zink, S. M. Seifermann, J. M. Navarro, T. Vitova, J. Göttlicher, R. Steininger, L. Weinhardt, M. Zimmer, M. Gerhards, C. Heske, S. Bräse, T. Baumann, D. Volz, *Chem. - Eur. J.* **2016**, *22*, 16400.
[20] S. V. Kunz, C. M. Cole, S. C. Gauci, F. Zaar, P. E. Shaw, C. S. K. Ranasinghe, T. Baumann, P. Sonar, S. D. Yambem, E. Blasco, C. Barner-Kowollik, J. P. Blinco, *Polym. Chem.* **2022**, *13*, 4241.
[21] I. Burgués-Ceballos, M. Stella, P. Lacharmoise, E. Martínez-Ferrero, *J. Mater. Chem. A* **2014**, *2*, 17711.
[22] L. Mu, Z. Hu, Z. Zhong, C. Jiang, J. Wang, J. Peng, Y. Cao, *Org. Electron.* **2017**, *51*, 308.
[23] D. Soltman, V. Subramanian, *Langmuir* **2008**, *24*, 2224.
[24] M. Hasan, S. Saggar, A. Shukla, F. Bencheikh, J. Sobus, S. K. M. Mcgregor, C. Adachi, S.-C. Lo, E. B. Namdas, *Nat. Commun.* **2022**, *13*, 254.
[25] W. H. Lee, D. H. Kim, P. Justin Jesuraj, H. Hafeez, J. C. Lee, D. K. Choi, T.-S. Bae, S. M. Yu, M. Song, C. S. Kim, S. Y. Ryu, *Mater. Res. Express* **2018**, *5*, 076201.

